Carbohydrate Polymers 282 (2022) 119126

Contents lists available at ScienceDirect

Carbohydrate Polymers

journal homepage: www.elsevier.com/locate/carbpol

Development and in vitro assessment of a bi-layered chitosan-nano-hydroxyapatite osteochondral scaffold

Katherine A. Pitrolino [a,**], Reda M. Felfel [b,c], Laura Macri Pellizzeri [a], Jane M[c]Laren [d], Alexander A. Popov [a,b], Virginie Sottile [a,e,*], Colin A. Scotchford [b], Brigitte E. Scammell [d], George A.F. Roberts [b], David M. Grant [b]

[a] Academic Unit Translational Medical Sciences, School of Medicine, University of Nottingham, UK
[b] Advanced Materials Research Group, Faculty of Engineering, University of Nottingham, UK
[c] Physics Department, Faculty of Science, Mansoura University, Mansoura 35516, Egypt
[d] Academic Unit Inflammation, Injury and Recovery Sciences, School of Medicine, University of Nottingham, UK
[e] Department of Molecular Medicine, University of Pavia, Italy

ARTICLE INFO

Keywords:
Chitosan
Osteochondral scaffold
Nano-hydroxyapatite
Graded porosity
Mesenchymal stem cells
Tissue engineering

ABSTRACT

An innovative approach was developed to engineer a multi-layered chitosan scaffold for osteochondral defect repair. A combination of freeze drying and porogen-leaching out methods produced a porous, bioresorbable scaffold with a distinct gradient of pore size (mean = 160–275 μm). Incorporation of 70 wt% nano-hydroxyapatite (nHA) provided additional strength to the bone-like layer. The scaffold showed instantaneous mechanical recovery under compressive loading and did not delaminate under tensile loading. The scaffold supported the attachment and proliferation of human mesenchymal stem cells (MSCs), with typical adherent cell morphology found on the bone layer compared to a rounded cell morphology on the chondrogenic layer. Osteogenic and chondrogenic differentiation of MSCs preferentially occurred in selected layers of the scaffold in vitro, driven by the distinct pore gradient and material composition. This scaffold is a suitable candidate for minimally invasive arthroscopic delivery in the clinic with potential to regenerate damaged cartilage and bone.

1. Introduction

Osteochondral tissue engineering has been extensively researched and possible solutions to musculoskeletal injuries, disease and age-related degeneration have been developed (Zou et al., 2016). Despite this focus, there is a lack of cost effective and scalable regenerative medicine options available for clinicians to treat osteochondral defects (Bicho et al., 2018). The ability of cartilage to lubricate bone movement and absorb mechanical loading is vital to a functioning articular joint, however it is a particularly problematic tissue to repair as it is aneural, avascular and contains a limited number of cells (chondrocytes). Cartilage defects often deteriorate, causing exposure of the underlying subchondral bone and osteochondral defects, including those caused by trauma and osteoarthritis, are a major burden on both the patient and the healthcare system (Kon et al., 2017). The pain linked to the loss of function in articulating joints reduces quality of life, decreases mobility, and may lead to other health conditions (King et al., 2017), adding to the substantial healthcare costs for these pathologies. Current strategies for pain relief and defect repair vary in complexity and may involve non-steroidal anti-inflammatories, debridement, microfracture and whole joint replacement (NICE, 2019). Whole joint replacement has a relatively limited lifespan as 1 in 20 need further surgery in 12 years (NHS, 2020). Compared to these therapeutic options, a tissue engineering approach seeking to intervene early and prevent further deterioration of a cartilage defect may provide an alternative, lifelong, and uniquely, a single treatment option. Such a large unmet clinical need calls for tissue engineered solutions to intervene early and prevent further deterioration of the defect, considering factors that facilitate cost-effective, large-scale manufacture as well as structural integrity and functional tissue regeneration.

Multi-layered osteochondral scaffolds made from synthetic or naturally derived materials including polysaccharides such as alginate or

* Correspondence to: V. Sottile, The University of Pavia, Via Ferrata 9, 27100 Pavia, Italy.
** Correspondence to: K.A. Pitrolino, The University of Nottingham, Room 312, Wolfson building, University Park, Nottingham NG7 2RD, UK.
E-mail addresses: KPitrolino@live.com (K.A. Pitrolino), virginie.sottile@unipv.it (V. Sottile).

https://doi.org/10.1016/j.carbpol.2022.119126
Received 14 October 2021; Received in revised form 4 January 2022; Accepted 7 January 2022
Available online 12 January 2022

carrageenan can guide tissue regeneration and facilitate functional repair (Reddy et al., 2021; Iglesias-Mejuto & García-González, 2021; Aslam Khan et al., 2020). The multi-layered properties, often defined by chemical composition and gradients of porosity, serve to mimic the natural architecture of an articulating joint, with biopolymers emerging as the preferred option over synthetic materials due to their natural biocompatibility (Xiao et al., 2019). Osteochondral devices entering early phase clinical trials are predominantly collagen-based devices, including CaRes (Schneider et al., 2011), MACI (Nawaz et al., 2014), MaioRegen (Kon et al., 2010), Chondro-Gide (McCarthy & Roberts, 2013), Osseofit (McCarrel et al., 2017) and Vericart (GlobeNewswire, 2018). Collagen, however, degrades at body temperature (Yan et al., 2010) and so is unlikely to provide support for tissue regeneration over the longer term. An alternative material to collagen is chitosan, a naturally derived long chain polysaccharide formed by deacetylation of naturally available chitin, a polymer of *N*-acetyl-D-glucosamine (Roberts, 1992) and a by-product of the shrimp industry (Yadav et al., 2019). Chitosan has a chemical structure similar to the glycoaminoglycans present in native cartilage tissue. It has properties of non-toxicity, biocompatibility, mucoadhesivity and biodegradability, which make it a suitable candidate for tissue engineering applications (Croisier & Jérôme, 2013; Busilacchi et al., 2013; Levengood & Zhang, 2014). Haemostatic properties of chitosan have been exploited for cartilage repair in commercial products such as BST-CarGel, developed for use in microfracture and mosaicplasty techniques (Stanish et al., 2013). In vivo preclinial trials of this hydrogel into femoral condyle defects of skeletally mature sheep showed restoration of glycosaminoglycan levels, increased cell proliferation and greater production of type II collagen compared to control defects using microfracture alone (Hoemann et al., 2005).

Bone tissue engineering has also been enhanced by the osteoconductive and osteoinductive properties of chitosan (Levengood & Zhang, 2014). Previous in vitro studies found that chitosan promoted the growth of calcium phosphate crystals, a precursor of bone hydroxyapatite (Costa-Pinto et al., 2008; Viala et al., 1996), and led to increased expression of alkaline phosphatase, a marker of early stage osteogenesis (Costa-Pinto et al., 2009). Animal studies showed evidence of freeze-dried chitosan sponges recruiting stem cells from the bone marrow, which led to mineralisation of a lesion in the femoral condyle of sheep (Muzzarelli et al., 1994), and 3D printed chitosan scaffolds were reported to promote regeneration of trabecular bone in a goat model (Zhang et al., 2017). The presence of a porous scaffold structure was particularly useful in bone repair as it allowed blood and nutrient flow and provided support for tissue regrowth (Muzzarelli et al., 1994). The addition of nHA rods to chitosan structures can increase compressive strength, enhance cell attachment and support osteogenesis (Oliveira et al., 2006; Malafaya & Reis, 2009). Combining chitosan with chemical cross-linkers can also improve the mechanical properties, and among existing cross-linked versions, chitosan-genipin gels have shown enhanced biocompatibility, mechanical strength and slower degradation rates when compared to chitosan-glutaraldehyde gels (Croisier & Jérôme, 2013).

Osteochondral scaffolds should exhibit mechanical resilience not only to meet the physical requirements of the joint, but also for their surgical implantation, which is increasingly performed via arthroscopic or minimally invasive delivery (Frank et al., 2019), and therefore they should exhibit mechanical properties compatible with the requirements of this surgical procedure. However, multi-layered tissue engineered scaffolds are prone to mechanical weakness at the interface between the layers, which can prevent tissue integration and limit functional repair (Martin et al., 2007; Zhang et al., 2020).

To address these limitations, the present study tested the hypothesis that a collagen-free tissue engineered scaffold with superior properties could be designed and manufactured using chitosan for the treatment of osteochondral lesions. The main objectives were to (1) use an innovative scalable manufacturing process to produce a chitosan-genipin multi-layered scaffold with controlled porosity in distinct but integrated layers, (2) assess the suitability of the scaffold for arthroscopic delivery by examining tensile strength, mechanical recovery, and delamination potential, (3) determine the effect of adding nHA rods to the bone layer, (4) ensure the device supports the proliferation of mesenchymal stem cells in both the cartilaginous and osseous phases.

2. Materials and methods

2.1. Materials

Chitosan powder (CS) from Weifeng Kehai Ltd, China with a molecular weight of 471 kDa and a degree of deacetylation of 84% ± 2%, glacial acetic acid (purity ≥ 99%) from Sigma-Aldrich, Dorset, UK, and Genipin (GN) from Guangxi Shanyun Biochemical Science and Technology Co. Ltd, China (98% purity) were used to prepare the stock aqueous solutions. Polycaprolactone (PCL) (MW: 14 kDa, purity > 99.5%), dichloromethane (DCM) (purity > 99.8%), polyvinyl alcohol (PVA, MW: 13–23 kDa, 87–89% hydrolysed), potassium hydroxide pellets (purity 85–99.95) and sodium borohydride solution (99%) were obtained from Sigma-Aldrich, Dorset, UK. Nano-hydroxyapatite rods (nHA, 0–40 nm diameter and 100–200 nm length) were used from a 14.5% (w/v) water suspension obtained from Promethean Particles Ltd, Nottingham, UK (Lester et al., 2013; Hui et al., 2018). Reagents used for cell culture including phosphate buffered saline (PBS), M Tris buffer, sodium phosphate (99%), cysteine hydrochloride (99%), EDTA were purchased from Thermo Fisher Scientific (Loughborough, UK).

2.2. Production of polycaprolactone (PCL) porogen microspheres

A PCL porogen was used to control the pore size gradient within the scaffold. The PCL porogen microparticles were produced using an emulsion method and two distinct size ranges were obtained using sieves to separate the required particle sizes.

The emulsion method involved making an emulsion stabiliser PVA/water solution and adding the PCL/DCM solution drop by drop to the stirred solution. A 0.3% polyvinyl alcohol (PVA) solution was prepared by dissolving 12 g of PVA in 1 L of distilled water at 95 °C with stirring at 500 rpm. This was then diluted down to 4 L and stirred at 300 rpm overnight. Any undissolved granules were filtered out. A solution of PCL was made by dissolving 25 g PCL (24% w/v) in 100 mL of DCM and added dropwise using a syringe pump set at 2 mL/min into the stirred solution of PVA at 300 rpm. The solution was continuously stirred overnight at room temperature so the DCM could fully evaporate and leave the PCL microspheres suspended in PVA solution. The microspheres were thoroughly washed in deionised water over filter paper before they were dried at 37 °C for 24 h. Finally, the PCL spheres were sieved, and 180–300 μm and 300–425 μm particles were collected for use in the scaffold production.

2.3. Production of chitosan-nHA composite scaffolds

A chitosan solution (4%) was prepared in distilled water with 2.5 v/v % glacial acetic acid and kept overnight to remove the trapped air bubbles. The scaffolds mixture was made by adding 4 mL of a 1% ethanoic solution of genipin with 10 g of PCL microspheres to 20 mL of CS solution. The first layer, containing PCL microspheres at a particle size range 300–425 μm, was cast and allowed to partially cross-link for 2 h before the second layer, containing PCL microspheres at a particle size range 180–300 μm, was cast on top. The bilayer structure was covered and allowed to further crosslink overnight before freezing at −20 °C for 24 h. The frozen structure was then transferred to a freeze dryer (Coolsafe 100-9 Pro) and left for at least 48 h to fully dehydrate. Individual scaffolds were cut from the mould using a 6 mm cork-borer and immersed in 2.5% alcoholic potassium hydroxide solution for 4 h at 50 °C to initiate the alkaline hydrolysis of the PCL microsphere ester

bonds. The PCL depolymerised and formed an ester salt (Tindall et al., 1994) leaving behind pores with a controlled size as shown in Fig. 1. The scaffolds were washed in methanol to remove any residual genipin and then repeatedly washed with distilled water to remove any residual salts from the depolymerisation process. The final processing stage involved immersing in 1% sodium borohydride/water solution for 24 h in a sealed container to remove the dark blue colour of the genipin cross-linker, washing in distilled water and then placing in a freeze dryer for 48 h. To produce the chitosan-nHA composite scaffold, a suspension of nHA rods was incorporated at 70% (w/w wrt CS) in the CS solution and PCL (300–425 μm) porogen mixture before cross-linking.

2.4. Characterisation of PCL porogen microspheres

Laser diffraction was used to determine the particle size distribution of the porogen microspheres. The two particle size ranges were analysed separately using a LS320 laser particle size analyser (Beckman Coulter Ltd, US), with a background flux measurement of 80,000. All readings were taken at a detector number of 20 and an obscurity between 8 and 12% to ensure a consistent concentration across samples.

2.5. Characterisation of scaffold pore size

For morphological analysis, the scaffold was mounted on sample plates using carbon adhesive cement (Agar scientific, Essex, UK) and sputter-coated with platinum for 80 s using a Polaron SC7640 (Quorum Technologies Ltd, Kent, United Kingdom) before imaging using scanning electron microscopy (SEM, Philips, XL30) with an accelerating voltage of 10 kV. The morphology of the scaffold was examined by environmental scanning electron microscopy SEM (eSEM) using a Quanta FEG 650 scanning electron microscope operating at 770 Pa. For pore size measurements, scaffolds were frozen overnight at −80 °C then fractured longitudinally to reveal the internal morphology, which was analysed using SEM. Each scaffold section was divided into three segments to allow measurement of the top, bottom and interphase. The pore size of the scaffold was determined from PenTabletDrive software (Huion Ltd, Shenzhen, China) by measuring the diameter of a minimum of 25 pores in three different areas of each scaffold layer (Siddiqui et al., 2015; Sarem et al., 2013) (Suppl. Fig. 1).

2.6. Mechanical properties and swelling properties of the scaffold

The mechanical properties of the chitosan scaffolds were determined using a compression-testing machine INSTRON 5966 (Instron Universal Testing Instruments, Buckinghamshire, UK) fitted with a 100 N load cell and set at 0.5 mm/min crosshead speed under ambient conditions, in accordance with ASTM 1621-10: 2010. The compression test was conducted on dry and wet scaffolds. Five scaffold samples (approximately 14 mm in length and 7 mm in diameter) were soaked in distilled water for 60 min and then tested applying 20% strain in each case. The scaffolds were briefly dried using tissue paper to avoid excess escape of water during testing. Strain was calculated from the compressive extension and compressive stress was calculated from the load data recorded from the equipment software using the accurate scaffold dimensions. Stress-strain curves were generated, and Young's modulus was calculated using the gradient of the stress/strain data within the linear region. Compressive strength was determined as the maximum compressive stress at 20% strain.

Mechanical recovery of the wet chitosan scaffolds was evaluated through the application of two successive cycles of compression test up to 70% strain at 0.5 mm/min. To examine the delamination resistance of the multi-layered scaffolds, individual dry samples were glued between two nylon rods (8 mm diameter and 30 mm length) using cyanoacrylate and left for 15 min to allow the glue to dry. The nylon rods were then clamped into the Instron, and tensile test was conducted at 0.5 mm/min until the scaffold failed. Tensile stress-strain curves and failure modes were recorded.

The impact of arthroscopic delivery on the performance of the scaffolds was analysed by a compressive test conducted on chitosan-nHA scaffolds prior and post-delivery through a clinical 6.5 × 75 mm threaded cannula (Stryker, Berkshire, UK). The scaffolds were radially compressed by approximately 30% of the initial diameter to be injected through the cannula.

The percentage of wet weight change was determined from the initial dry and wet weight of each scaffold using the formula below. The scaffolds were dried under vacuum at 50 °C for at least 2 h to determine the initial dry weight (W_o) and the wet weight (W_w) was determined by pre-blotting to remove excess water as previously described (Siddiqui et al., 2015):

$$\frac{W_w - W_o}{W_o} \times 100 \quad (1)$$

The swelling ratio was evaluated after immersion of the cylindrical scaffolds (14 mm × 7 mm) in phosphate buffered saline (PBS) (Sigma-Aldrich, Dorset, UK) for 30 h at 37 °C using the following formula (Pati et al., 2012):

$$\frac{W_f - W_o}{W_o} \quad (2)$$

where W_f is the final wet weight of the scaffold. The final figures were normalised to account for the increased weight of the chitosan-nHA scaffold.

2.7. Degradation properties of scaffold

Scaffold degradation properties were tested according to BS ISO 13781. Five dry cylindrical scaffolds, approximately 0.04 g in weight and 14 mm height and 7 mm in diameter, were submersed individually in capped glass vials containing 20 mL of PBS, stored at 37 °C and tested at regular intervals (0, 3, 7, 14, 21 days) for weight loss and mechanical properties. The mechanical properties were tested according to the method described in section 2.6. The initial weight (W_o) of each scaffold was taken both wet and dry. At each time point the wet weight of the scaffolds was taken after at least 2 h immersion in PBS. Excess water was

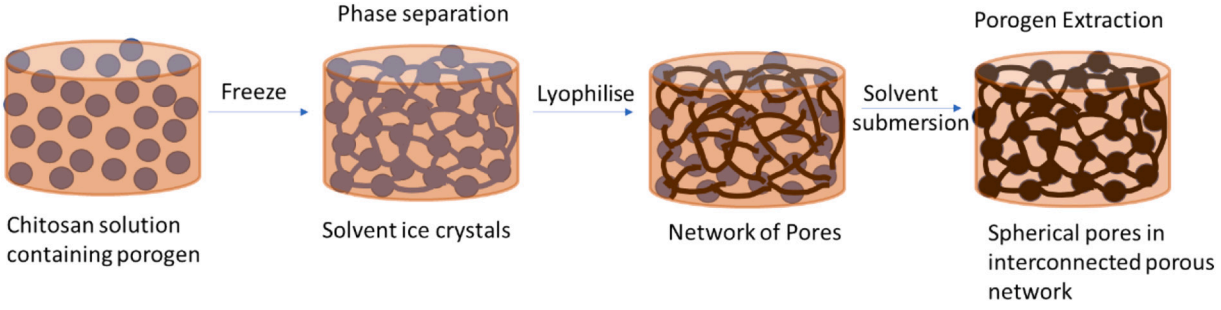

Fig. 1. Schematic of scaffold production using freeze drying and particulate leaching methods.

first removed by blotting the scaffold with tissue paper. The scaffolds were dried under vacuum at 50 °C for at least 2 h to determine the dry weight (W_t) at each time point (Siddiqui et al., 2015).

The percentage of mass loss was calculated using the following equation:

$$\frac{W_o - W_t}{W_o} \times 100 \quad (3)$$

2.8. Cell culture

Immortalised bone marrow-derived human mesenchymal stem cells (MSCs) (France et al., 2014) labelled with the green fluorescent protein were cultured as previously described (Harrison et al., 2017). Briefly, the standard growth medium used was Dulbecco's Modified Eagle's Medium (DMEM) supplemented with 10% (v/v) foetal bovine serum (FBS), 1% (v/v) non-essential amino acids, 1% (v/v) L-glutamine, and 0.5% (v/v) antibiotic/antimycotics mixture consisting of 100 units/mL penicillin, 0.1 mg/mL streptomycin and 0.25 μg/mL amphotericin B in media working concentration and changed every 2–3 days. The cells were passaged using 0.25% trypsin/0.02% EDTA and maintained at 37 °C in 5% CO_2.

2.9. Cell metabolic activity

For metabolic activity and DNA tests, a 14 mm scaffold cylinder was used. After alcohol sterilisation and extensive washes, scaffolds were seeded with 1 mL of a 10^6 cells/mL cell suspension and incubated in standard growth medium. The metabolic activity of the attached cells was measured at 48 h after exposure to the supernatant using a PrestoBlue kit according to the manufacturer's instruction. The scaffold was seeded with stem cells at a cell density of 1 Million cells per mL. Briefly, after 50 min incubation, 100 L samples were collected from each well and transferred in triplicate to a 96-well plate. The fluorescence intensity was measured using a TECAN Infinite M200 plate reader (Tecan Trading AG, Switzerland) at 560 nm excitation and 590 nm emission with a constant gain of 85% determined from previous experiments.

2.10. Cell DNA content

The cells were lysed using a freeze/thaw method and analysed for DNA content using the QuantIT PicoGreen assay kit (Thermo Fisher Scientific, UK) according to the manufacturer's instructions. Briefly, the plate containing 100 μL of cell lysate was incubated at room temperature in the dark for 5 min with an equal volume of PicoGreen reagent before reading on a plate reader at 480 nm excitation and 520 nm emission. The fluorescence readings were quantified into DNA content using a DNA standard curve prepared from the Lambda virus DNA provided in the kit. The fluorescence readings were quantified into DNA content. Imaging of live cells was performed using a JuLI FL imaging microscope and stage (Nano EnTek Inc., Seoul, Korea) and a Nikon Eclipse Ts2-FL inverted microscope (Nikon UK Ltd, Surrey, UK).

2.11. Cell differentiation

Differentiation medium was used to selectively direct the differentiation of the seeded stem cells toward an osteogenic or chondrogenic lineage. For all differentiation experiments, 2 mm slices were cut from a whole scaffold cylinder, seeded with 500 μL of 0.8 M cells/mL cell suspension, incubated in standard growth medium and at day 2 the medium was replaced with differentiation medium. The media was refreshed every 2–3 days. Osteogenic culture was maintained for 21 days using standard growth medium supplemented with 0.1 μM dexamethasone, 50 μM L-ascorbic acid and 10 mM β-glycerophosphate (Sigma-Aldrich, Dorset, UK). Chondrogenic culture was maintained for 35 days using standard growth medium supplemented with 0.1 μM Dexamethasone, 50 μM L-ascorbic acid, 40 μg/mL Proline, 1 × ITS (Sigma-Aldrich, Dorset, UK) and 10 ng/mL TGF-β (Thermo Fisher Scientific, UK).

2.12. Alkaline phosphatase assay

Early-stage osteogenesis was assessed by measuring alkaline phosphatase (ALP) activity using a Sigmafast kit (Sigma-Aldrich, Dorset, UK). Briefly, a 4.5 mM *p*-nitrophenyl phosphate solution was made up in 0.2 M Tris buffer (Sigma-Aldrich) and 500 μL was added to each scaffold well. After 20 minute incubation in the dark at room temperature, 100 μL of solution was transferred in triplicate to a 96 well plate and the optical density was read at 405 nm absorbance on a Tecan micro-plate reader.

2.13. DMMB assay

A 1,9-dimethylmethylene blue (DMMB) assay was used to quantify the increased level of sulphated glycosaminoglycans (GAGs) present on chitosan-nHA scaffolds after chondrogenic differentiation of MSCs. The scaffolds were prepared by transferring 2 mm slices of each layer into Eppendorf tubes on dry ice, flash freezing in liquid nitrogen and storing at -80 °C until needed. On thawing, the slices were finely minced using a pair of surgical scissors and 1 mL of 0.01% papain solution (Sigma-Aldrich, Dorset, Ltd) was added in papain buffer (0.1 M sodium phosphate, 0.005 M cysteine hydrochloride and 0.005 M EDTA, pH 7.5, Sigma-Aldrich) to dissociate the GAGs from the scaffold matrix and other glycoproteins. After mixing with papain buffer, the scaffolds were incubated at 65 °C for at least 18 h. The digested scaffolds were centrifuged at 10,000*g* for 10 min and the supernatant was analysed with a Blyscan sGAG Assay Kit (Biocolor Ltd, County Antrim, UK). Briefly, dye reagent was added to each tube and mixed for 30 min on a plate shaker before centrifugation at 12,000 rpm for 10 min. The pellet was resuspended in dissociation reagent, vortexed and centrifuged at 12,000 rpm for 5 min before 200 μL was transferred in duplicate into a 96 well plate. Absorbance values were read at 656 nm using a Tecan micro-plate reader. Quantification of sulphated GAGs was obtained using a 1–5 μg chondroitin sulphate standard curve contained within the kit.

2.14. Statistical analysis

At least five replicates ($n \geq 5$) of each specimen were used in all tests and the obtained results are represented as mean ± SEM (standard error of the mean), unless otherwise mentioned. All graphs and statistical analyses were performed using GraphPad Prism 6.0. One-way ANOVA analysis with a post hoc Tukey comparison was applied for mechanical and degradation tests. For cytotoxicity, the data was analysed using two-way ANOVA with Tukey post hoc testing for multiple comparisons and the statistical difference between conditions is shown, with p values as * ≤ 0.05, ** ≤ 0.01, *** ≤ 0.001, **** ≤ 0.0001.

3. Results

3.1. Production of chitosan scaffolds

A schematic diagram of the scaffold manufacturing process is shown in Fig. 1. The size of the pores in each of the two scaffold parts was controlled by adding sieved fractions of a porogen of PCL microspheres. Careful control of the crosslinking conditions ensured there was adequate integration of the two layers at the interface and an interconnected network of pores was achieved by freeze drying. Size distribution by laser diffraction of the PCL microspheres is shown in Fig. 2, 98% of the particles in the sieve range 180–300 μm were within this range limit, with a mean particle size of 238 μm. The size distribution graph for the larger size range, 300–425 μm showed 81% of the particles

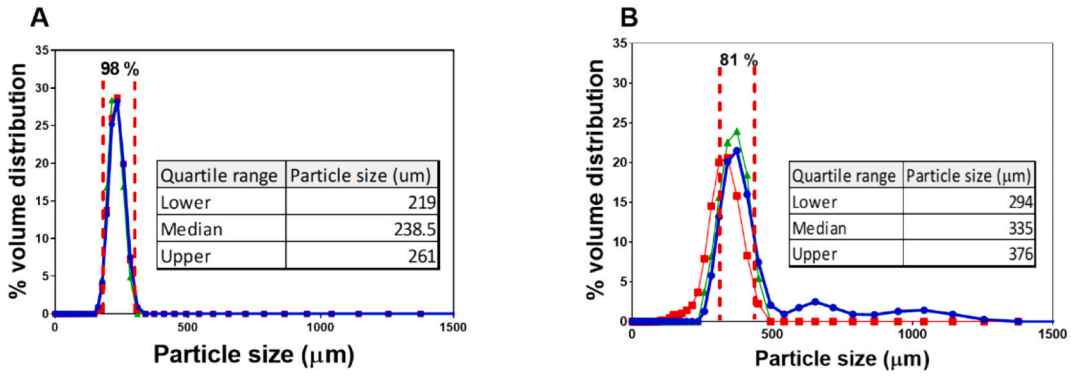

Fig. 2. Size distribution determined by laser diffraction of PLC microspheres within the two particle size ranges 180–300 μm (A) and 300–450 μm (B). Red dashed lines indicate the sieve size ranges used to determine the particle size ranges. Three samples were used, shown individually by red, blue and green filled lines. More than 98% of the particles are within the 180 and 300 μm size range with a mean particle size of 238 μm, n = 3. More than 81% of the particles are within the 300 and 425 μm size range with a mean particle size of 335 μm, n = 3.

within this size range, with a mean particle size of 335 μm.

3.2. Production of chitosan-nHA composite scaffolds

FTIR spectra taken from the scaffold prior to and post porogen removal treatment confirmed the removal of the PCL porogen (Suppl. Fig. 2). SEM images of the internal pore structure of the scaffolds detailing the large and small pore size regions of scaffold are shown in Fig. 3A and B, alongside an image of a longitudinal cross-section of the bilayer scaffold (Fig. 3D). The images show interconnected, round shaped pores evenly distributed throughout the scaffold. Pore size distribution is shown in Fig. 3C and details a mean pore size of 275 μm for the large pore (subchondral) region, a mean pore size of 248 μm at the interface between the two layers and a mean pore size of 160 μm in the small pore region. This size distribution resulted in an overall porosity of ca. 92%, determined using an Archimedes method (Hughes, 2005).

To improve the mechanical performance and cell adherence as well as provide a direct cue for osteoinduction, nHA rods were incorporated

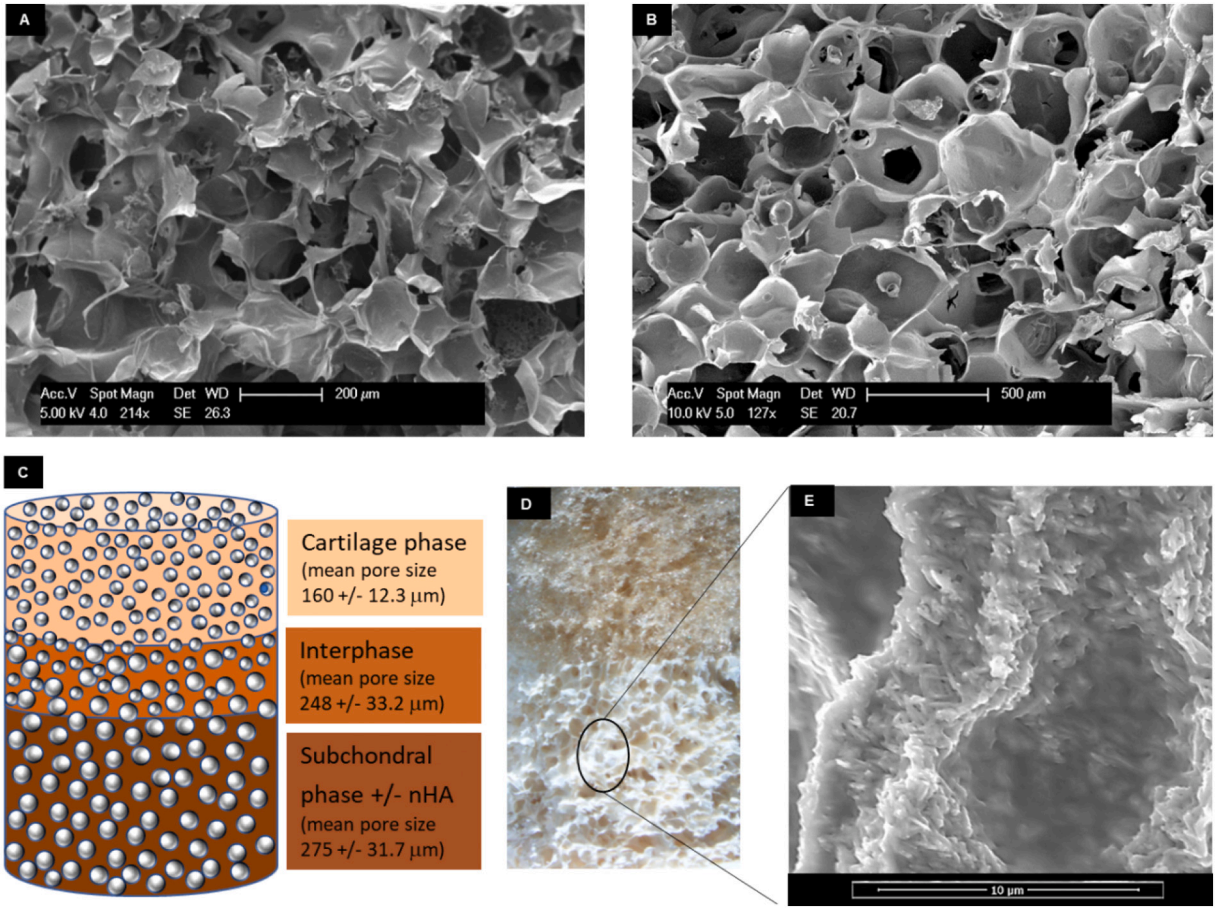

Fig. 3. SEM images showing a rigid internal pore structure of the composite scaffolds in the cartilage (A, chitosan) and bone (B, chitosan-nHA) phases. A schematic image of the scaffold (C) shows the mean pore size in each phase, and an optical image of the scaffold (D) shows the nHA layer on the bottom. An eSEM image showing the distribution and structure of nHA rods incorporated into the scaffold structure is shown in (E).

into the bone-like layer of the chitosan scaffold, as shown in Fig. 3B. The distribution and structure of nHA rods on the chitosan-nHA composite scaffold is displayed in Fig. 3E and was confirmed by energy dispersive X-ray (EDX) surface analysis performed on the scaffolds, which showed calcium and phosphorus present on the surface of chitosan-nHA scaffold, while it was undetected on the chitosan-only sample (Suppl. Fig. 3). Rods homogeneously distributed over the entire scaffold structure produced a more rigid internal architecture resulting in wider pore struts, measuring more than 10 μm thick, and more defined rounded pores than the cartilage-like layer. MicroCT analysis of the scaffold confirmed the porous structure with differential pore size across the scaffold (Suppl. Fig. 4) and the absence of a tide mark at the interphase as seen by SEM (Suppl. Fig. 5). Analysis of microCT data (Suppl. Fig. 4) confirmed high open porosity in both the large pore section (71.79% ± 3.84) and small pore section (86.28% ± 3.99).

3.3. Mechanical and swelling properties of the scaffold

The mechanical and swelling properties of both the chitosan and chitosan-nHA scaffolds were analysed independently as shown in Fig. 4. The wet weight of both scaffolds increased quickly in the first hour of immersion in PBS, see Fig. 4A, before reaching the saturation after 4 h. The addition of nHA rods had no significant effect on the swelling ratio once the figures were normalised for the increased initial weight of the chitosan-nHA scaffold, as displayed in Fig. 4B, the chitosan-nHA scaffold had a mean ratio of 8.3 (±0.2) compared to a mean ratio of 8.6 (±0.2) for the chitosan-only scaffold.

The compressive strength of the hydrated chitosan-nHA composite, as displayed in Fig. 4C, shows a 2-fold increase in strength with the addition of nHA resulting in a value of 4.81 (±0.79) kPa compared to 2.33 (±0.06) kPa for the chitosan-only scaffold. The compressive modulus follows the same trend with the chitosan-nHA composite scaffold (34.2 ± 2.7 kPa) displaying a significantly higher modulus than the chitosan-only scaffold (18.6 ± 0.8 kPa) as detailed in Fig. 4D.

3.4. Scaffold degradation, mechanical retention, and delamination properties

The chitosan-nHA scaffold was chosen for further in vitro studies, including degradation and mechanical retention tests, due to its increased mechanical properties. Tensile tests to examine the delamination potential of the composite scaffold were also performed. Fig. 5A shows that the chitosan-nHA composite scaffold had a low rate of mass loss under the degradation tests, with only 5% mass loss after 21 days of submersion in PBS. This was consistent with the scaffold retaining compressive strength and modulus during the early stages of degradation as shown in Fig. 5B and C. Indeed, an increase in both compressive strength and modulus was seen after the initial time-point (day 3). Dry scaffolds had compressive strength and modulus of 100 kPa and 1600 kPa, respectively.

Under tensile loading, the chitosan-nHA scaffolds exhibited a gradual ductile failure mode initiated in the chitosan-only region away from the interface.

When exposed to repeated compressive loads of up to 70% strain, the wet scaffolds exhibited instantaneous mechanical recovery (Fig. 6A). The compressive stress-strain graphs for the scaffold at repeated cycles of 70% strain, as shown in Fig. 6, show strong similarity, indicating preservation of mechanical properties, see Supplementary Video 1. This suggested applicability for possible arthroscopic delivery to the joint in vivo, which was investigated further by testing the compressive strength of the chitosan-nHA scaffolds prior and post-delivery through a clinical cannula (Fig. 6B, C & D), see Supplementary Video 2. No significant change in compressive properties of the scaffolds was detected due to the injection process.

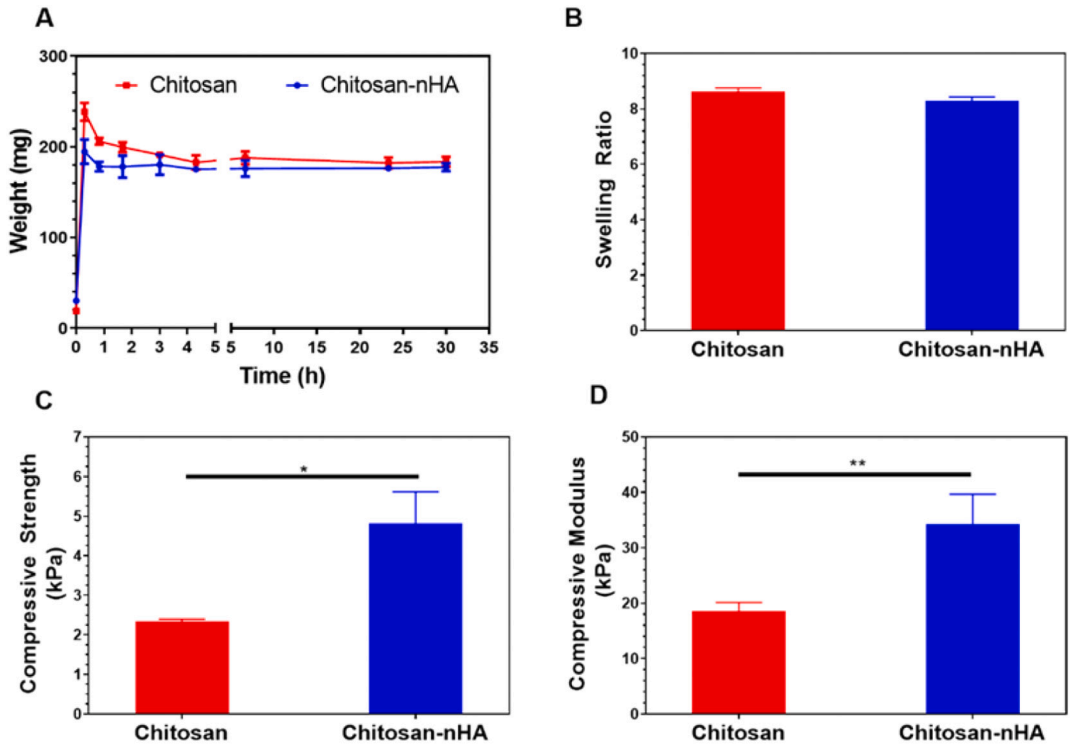

Fig. 4. Mechanical properties and swelling of chitosan-only and chitosan-nHA composite scaffolds. The weight (A) and normalised swelling ratio at 30 h for both scaffolds (B) showed no significant difference. However, the compressive strength (C) and modulus (D) were significantly increased in chitosan-nHA composite scaffolds compared to chitosan-only scaffolds. Results are expressed as mean ± standard error of the mean, n = 3. Data was analysed using an unpaired *t*-test, adjusted p values, * ≤ 0.05, ** ≤ 0.005.

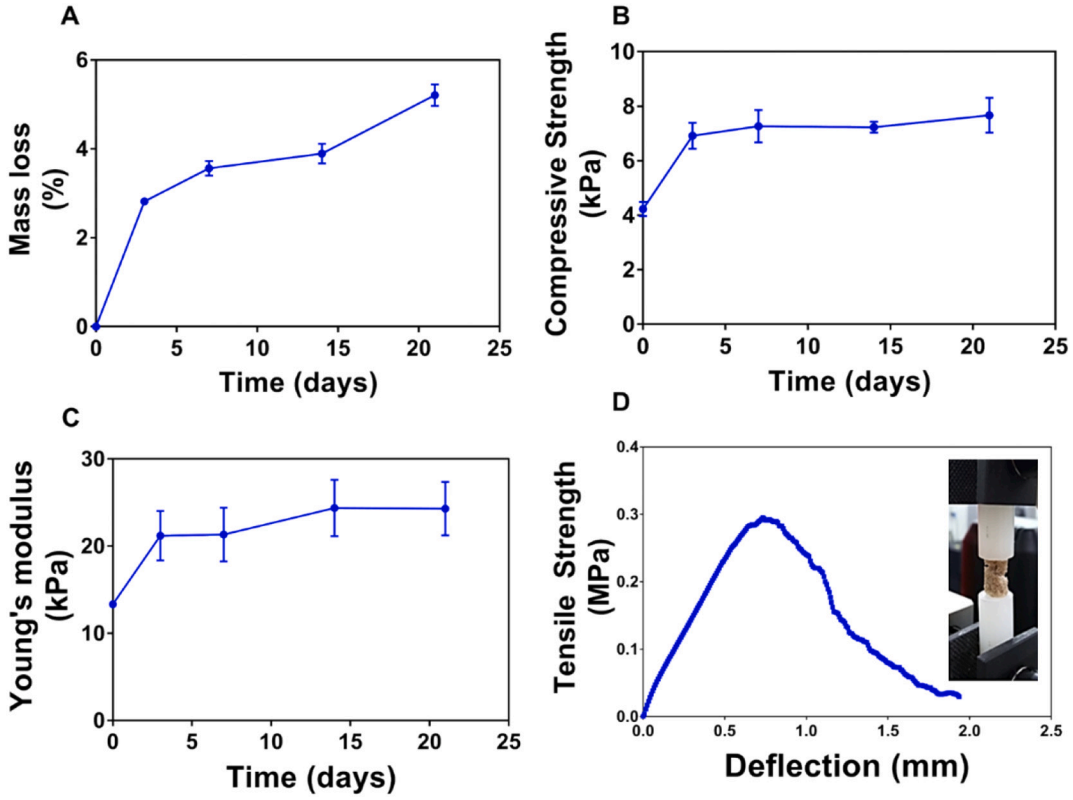

Fig. 5. Mass loss, mechanical retention, and delamination profile of chitosan-nHA composite scaffolds monitored after incubation over 21 days in PBS at 37 °C. A) Mass loss over time, B) mechanical strength, C) mechanical modulus of scaffolds at time points up to 21 days after immersion in PBS solution. D) shows the scaffolds ability to maintain a strong interface under tensile load. Results are expressed as the mean ± standard error of the mean, n = 5.

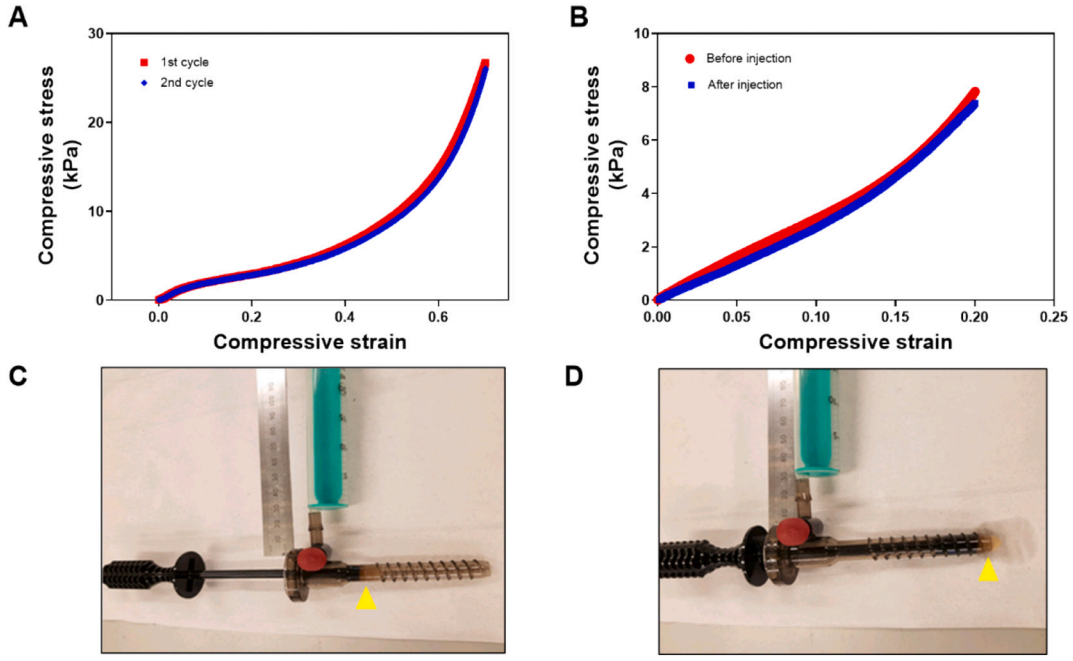

Fig. 6. (A) Mechanical recovery from two successive cycles of compressive stress–strain up to 70% strain and (B) stress-strain curves before and after simulated delivery through an arthroscopic cannula (C, D) of chitosan-nHA composite scaffolds. The yellow arrow indicates the position of the scaffold before (C) and after (D) delivery.

3.5. Scaffold cytocompatibility - cell metabolic activity and DNA content

The biological properties of the chitosan-only and chitosan-nHA scaffolds were examined by seeding each scaffold with MSCs and analysing cell growth. Tests with MSCs showed that cell colonisation was enhanced on chitosan-nHA composite scaffolds, with nearly double the

metabolic activity for cell-seeded chitosan-nHA scaffolds when compared to chitosan-only scaffolds at day 2 (Fig. 7A). Similarly, Fig. 7B shows a significant increase in the DNA content for cell-seeded chitosan-nHA composite scaffolds when compared to chitosan-only scaffolds, indicating higher cell content. SEM imaging at day 2 after MSC seeding showed cell adherence to the material (Suppl. Fig. 6), with cell sheets visibly attached to chitosan-nHA composite compared to more rounded cell clusters present on chitosan-only scaffolds (Fig. 7C and D).

3.6. Scaffold support for stem cell differentiation

Culture protocols were applied to promote the differentiation of stem cells to the osteogenic and chondrogenic lineage. A confocal imaging scan performed on seeded scaffolds confirmed the presence of cells within the structure at day 11 (Suppl. Fig. 7 and Suppl. Videos 3 & 4). When osteogenic differentiation medium was added to cells on both scaffolds, there was a significant increase in alkaline phosphatase (ALP) activity when compared to cells cultured on scaffolds in standard medium at day 14 as shown in Fig. 8A. There was also an increase in ALP activity from day 7 to day 14 followed by a significant decline at day 21 for cells cultured in osteogenic medium on both scaffolds (Fig. 8A). There was no significant difference between the 2 types of scaffolds (Fig. 8A), indicating that both types of scaffolds can support early-stage MSC osteogenesis.

Fluorescent microscope imaging of MSC-seeded chitosan-nHA scaffolds (Fig. 8C and D) showed clusters of cells bridging pores after 14 days in standard medium (C), while in osteogenic medium (D), cell sheets were observed to cover large areas of the scaffold topography. Von Kossa staining after 21 days confirmed the differentiation response of cells seeded on scaffolds under osteogenic conditions (Suppl. Fig. 8).

When MSC-seeded scaffolds were exposed to chondrogenic differentiation medium, both types of chitosan surface showed an increase in GAG content at day 35 compared to standard medium, however significantly more GAGs were detected on the chitosan-only layer of the scaffold compared the chitosan-nHA layer (Fig. 8B). The final content of GAGs detected in the chitosan-only scaffold was double the final content detected in the chitosan-nHA scaffold.

4. Discussion

4.1. Characterisation of scaffold pore size and porosity

The degree of cross-linking, the freeze-drying conditions, and the addition of a porogen determined the final pore size, interconnected network and porosity of the scaffolds produced here. The bilayer scaffold structure was stratified by pore size, using two different porogen size distributions to create two distinct layers. An analysis of these size ranges found both small and large sized porogen microspheres predominantly within the desired specifications, confirming the effectiveness of the microsphere production method. When comparing the pore size measured from SEM images to the porogen size analysis, a lower mean pore size was seen in the large and small regions as well as the interface. This could be expected as the processes of dehydration/freeze-drying of the scaffold after removal of the porogen, in preparation for SEM, can lead to shrinkage. Smaller pores, created by solvent sublimation during freeze drying, would also contribute to a reduction in the overall scaffold mean pore size (Levengood & Zhang, 2014).

The scaffolds had both a macro and micro porous structure based on the pore size measurements, which is considered beneficial for initial cell attachment and growth for osteoblasts (Nath et al., 2015), and for providing a sufficiently porous structure to allow transfer of nutrients and waste (Hutmacher, 2000). Previous reports used scaffolds for cell

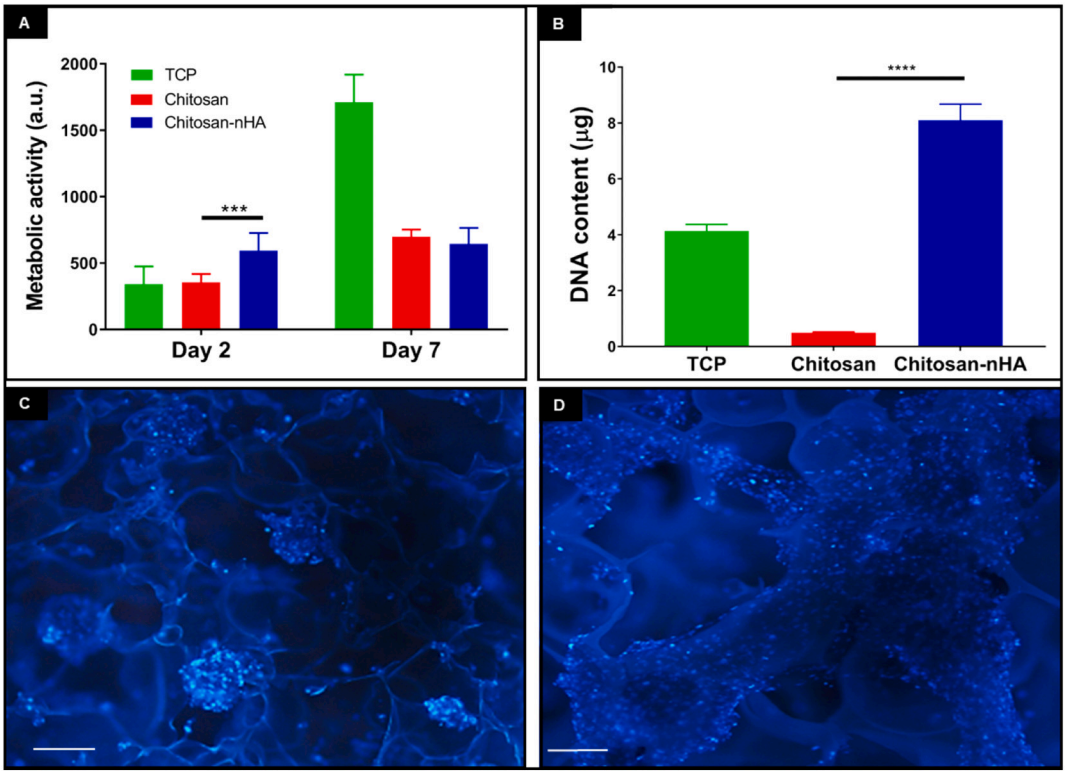

Fig. 7. Cell growth on chitosan scaffolds. Metabolic activity (A) and DNA content (B) for MSCs seeded onto chitosan-nHA composite scaffolds and chitosan-only scaffolds at day 2 and day 7 of culture. Both scaffolds were compared to the cell response on a tissue culture plastic (TCP) control. Results are expressed as mean ± standard error of the mean, n = 5. Data was analysed using one-way ANOVA with Tukey's post hoc testing for multiple comparisons, adjusted p values, *** ≤ 0.001, **** ≤ 0.0001. Fluorescent images of Hoechst-stained nuclei of MSCs seeded onto the chitosan-only (C) and chitosan-nHA composite (D) scaffolds at day 2 post-seeding. Scale bar shows 250 μm.

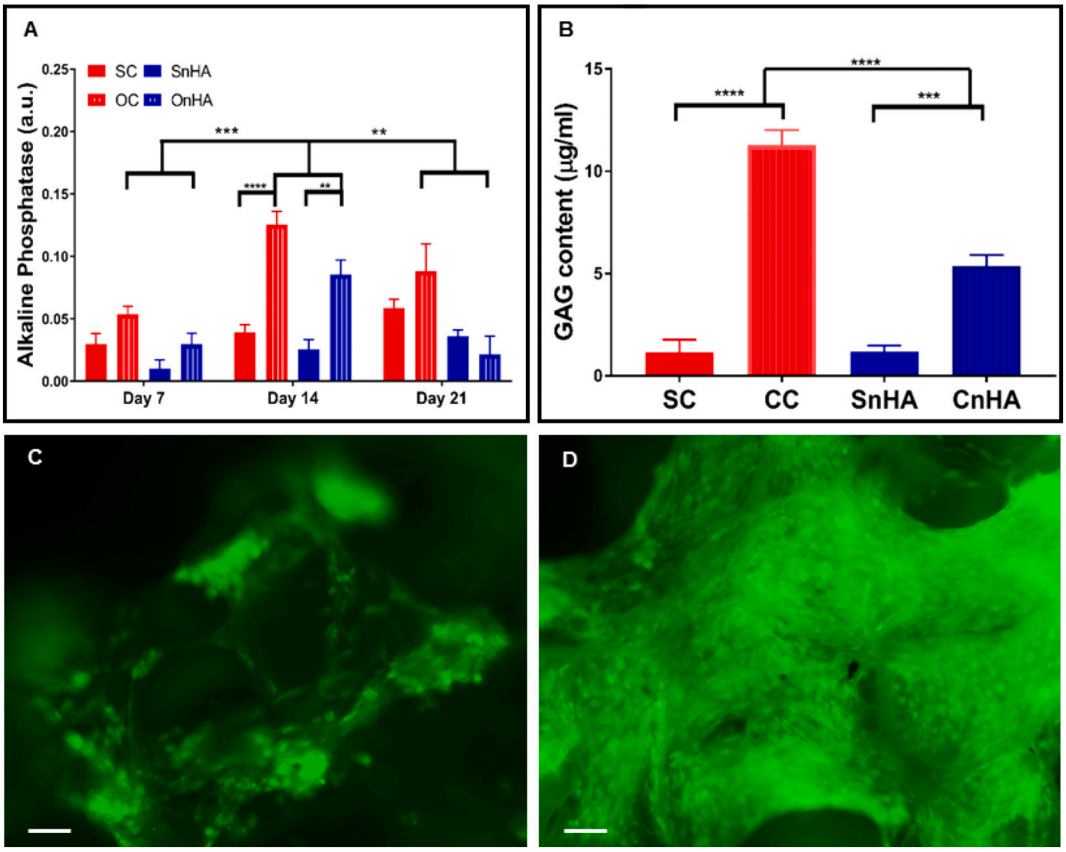

Fig. 8. Cell differentiation on chitosan scaffolds. Alkaline phosphatase activity (A) and sulphated glycosaminoglycans (B) measured in MSC-seeded chitosan scaffolds exposed to osteogenic and chondrogenic culture conditions, respectively. GAG content was measured at day 35 of culture in chondrogenic medium. (SC = chitosan scaffold in standard culture, OC = chitosan scaffold in osteogenic medium, CC = chitosan scaffold in chondrogenic medium, SnHA = chitosan-nHA scaffold in standard culture, OnHA = chitosan-nHA scaffold in osteogenic medium, CnHA = chitosan-nHA scaffold in chondrogenic medium, a.u. = absorbance units.) Results are expressed as mean ± standard error of the mean, n = 5. Data was analysed using one-way ANOVA with Tukey's post hoc testing for multiple comparisons, adjusted p values, ** ≤ 0.01, *** ≤ 0.001, **** ≤ 0.0001. Fluorescent microscopy showing MSCs seeded onto chitosan-nHA composite scaffolds, after 14 days in standard culture (C) and osteogenic medium (D). Scale bar shows 100 µm.

culture trials that had similar particle size ranges to the present study and reported a positive cell response using mesenchymal stem cells (Siddiqui et al., 2015), an osteoblast cell line (Yan et al., 2010), and rabbit chondrocytes (Nath et al., 2015). Other work has highlighted the need to tailor the pore size to the specific cell type after observing that osteoblasts and MSCs differ in their response to a particular pore size on a collagen-glycoaminoglycan scaffold (Murphy et al., 2016). It therefore could be useful to examine how osteoblasts and chondrocytes react to the chitosan surface and determine whether cell attachment and proliferation could be further optimised based on pore size.

4.2. *Mechanical and swelling properties of the scaffolds*

Both the chitosan-only and the chitosan-nHA composite scaffold had a strong ability to absorb water. This capacity indicates the scaffold would be beneficial for biomedical applications as swelling increases the porosity and the surface area for cell attachment and tissue regeneration (Levengood & Zhang, 2014). In this case, swelling was enhanced by the presence of chitosan's hydrophilic groups, and the stability and presence of a porous network allowing the scaffold to absorb water and increase in volume. Chitosan is naturally hydrophilic due to the presence of free amino and hydroxyl groups that are distributed throughout the polymer chain, which explains the high swelling ability of both scaffold types produced in this study, as reported in other studies with genipin-crosslinked chitosan scaffolds (Sarem et al., 2013; Nath et al., 2015; Siddiqui et al., 2015; Yan et al., 2010).

The addition of nHA rods to the scaffold increased the compressive strength by almost 50% when compared to the same scaffold without nHA, which is also in line with previous studies, although the specific values vary between research groups (Oliveira et al., 2006; Malafaya & Reis, 2009; Moreau & Xu, 2009). This variation is due to the concentrations of the materials used, method of manufacture, final porosity of the scaffold and the testing method used. For example, while similar bilayer scaffolds exhibited the same 50% increase in strength from the HA-containing to HA-free scaffolds, the actual values were several magnitudes higher than those reported in the present study due to the decrease in porosity formed by combining chitosan with sintered HA particles (Malafaya & Reis, 2009). Similar values of compressive modulus to those in this study (34.2 ± 2.7 kPa), were recorded by another group that used 2% chitosan solution and 1% wt HA (9.2 ± 0.2 kPa) and measured the scaffold in the hydrated state (Thein-Han & Misra, 2009).

While the compressive strength and modulus values obtained were not equivalent to those found in native tissue, as shown in Table 1, this is comparable to many other natural biopolymer scaffolds (Reddy et al., 2021; Thein-Han & Misra, 2009). The exact values desired for a tissue-engineered scaffold are not clear from the literature (Hutmacher, 2000; Harley et al., 2010). Some work suggests it is not necessary to mimic the mechanical strength of the native tissue (Harley et al., 2010) but instead concentrate on creating the right cell niche for the cells to proliferate and differentiate into functional tissue. For example, synthetic biopolymer scaffolds have a mechanical strength more representative of hard tissue, however, they often have poor cell binding ability (Reddy et al., 2021). It may also be more important for the scaffold to bend and

Table 1
Comparison of compressive strength and modulus for native tissue and natural biopolymer scaffolds.

Material	Compressive strength (MPa)	Young's Modulus (kPa)	Ref
Cortical bone	130–180	1.2×10^7–1.8×10^7	(Harley et al., 2010)
Cancellous Bone	4–12	100,000–500,000	
Articular cartilage	0.15–0.35	500–700	
Chitosan-only scaffold	0.00233	18.6 ± 0.2	This study
Chitosan-nHA composite scaffold	0.00481	34.2 ± 2.7	This study
Chitosan-only scaffold	Not recorded	9.2 ± 0.2	(Thein-Han & Misra, 2009)
Chitosan-nHA composite scaffold	Not recorded	6.0 ± 0.3	(Thein-Han & Misra, 2009)

Information gathered from Harley et al. (2010) and Thein-Han & Misra (2009).

yield under pressure in vivo as this may convey mechanical forces to the neighbouring stem cells and help to stimulate osteoblast and chondrocyte formation via mechanotransduction (Harley et al., 2010). Since the properties of a cell-seeded scaffold will change as the scaffold is progressively colonised and integrates with the surrounding tissue, an initial low compressive strength of the starting material may not be an issue to achieve long term repair.

4.3. Scaffold degradation, mechanical retention, and delamination properties

The mass loss over time observed for the chitosan-nHA scaffold showed a relatively slow degradation rate, with only a 5% reduction in weight after 3 weeks. This is attributed to multiple factors, including a high degree of deacetylation in the chitosan (DD 84%) (Vårum et al., 1997) used in this study, the crosslinking action of genipin, and the presence of nHA rods. The rate slowed after the initial time point, which is consistent with the fact that chitosan degrades by hydrolysis using bulk erosion mechanisms (Ren et al., 2005; Dang et al., 2011).

The compressive strength and modulus of the scaffolds at day 0 were significantly decreased from 100 and 1600 kPa (for dry scaffolds) to 4 kPa and 13 kPa after hydration in PBS for 60 min. This was expected due to the plasticisation effect of the water (Felfel et al., 2018). However, the mechanical properties were retained during the degradation process and indeed an increase in compressive modulus was observed at day 3, which was attributed to the increase in swelling of the scaffold. Swelling-strengthening and swelling-stiffening effects have been reported in the literature for scaffolds and hydrogels (Felfel et al., 2018; Offeddu et al., 2018; Wu et al., 2020). A key consideration for clinical use is how the in vivo environment may differ from the in vitro model used in this study, for instance through different pH conditions and possible effects on degradation rates (Felfel et al., 2018). Acidic degradation media mimicking inflamed tissue was reported to accelerate the degradation of the scaffolds (Felfel et al., 2018), and it will be interesting to examine how physiological parameters such as simulated body fluid and enzymes present in tissues may affect the degradation of chitosan scaffolds (Ren et al., 2005).

All stress/strain graphs, produced using hydrated chitosan-nHA scaffolds, followed the pattern of a porous material (Gibson & Ashby, 1997), with an initial linear region demonstrating elastic deformation of the pore walls then a plateau in stress as the cell walls start to collapse, and a final increase as the material densifies following progressive compressing of the pores.

The scaffold exhibited excellent mechanical recovery characteristics, as the structure returned instantaneously to its original shape and size after experiencing both 70% compressive strain and after being injected through a clinical cannula which was repeated several times. This mechanical recovery after compression supports the scaffold's suitability in the clinic for minimally invasive arthroscopic delivery, which would potentially reduce the associated pain, recovery time and cost for patients after surgery.

Although the scaffold contained two distinctive porous layers there was no evidence of delamination at the interface, during handling or after the compression tests. This has significant advantages over unconnected or poorly connected bilayer or trilayer structures that are likely to suffer from delamination when subjected to mechanical challenges such as arthroscopic delivery and the stresses found naturally in the joint (Zhang et al., 2020). Therefore, a strong interface which mimics the tidemark of the articular joint with a gradual transition between layers is considered an advantage in the clinic (Martin et al., 2007). The chitosan/chitosan-nHA scaffold structure also exhibited a distinct pore gradient mimicking the material transitions present in the native osteochondral tissue, which is not currently achieved in products affixing independent chondral or bone phases (Harley et al., 2010; Zhang et al., 2020).

When the scaffold was placed under tensile load, the structure failed by ductile failure however it did not delaminate at the interface, indicating the continuous strong bonding and a robust pore gradient within the composite developed by the manufacturing process. The tensile failure was initiated at one of the pores and then propagated until the scaffold failed under tension. The tensile failure stress was 0.36 ± 0.07, however, such tensile forces are unlikely to be experienced in the physiological environment of osteochondral tissue, (Harley et al., 2010), so this property will be clinically relevant only when considering the scaffold's robustness during handling and implantation.

4.4. Scaffold cytocompatibility – cell metabolic activity and DNA content

As well as increased strength, the addition of HA to tissue engineered scaffolds has been observed to be osteoconductive and osteoinductive, both supporting the integration of the scaffold with the surrounding bone tissue and mediating osteogenesis (Gil Mur, 2016). When incorporating nHA rods into the chitosan scaffold developed in this study, the metabolic activity and DNA content of MSC-seeded scaffolds showed a significant increase at early timepoints. An enhanced cell response to HA has also been reported with MC 3T3-E1 cells (Beşkardeş et al., 2015; Kong et al., 2005; Thein-Han & Misra, 2009) and bone marrow stem cells from animal (Moreau & Xu, 2009; Oliveira et al., 2006), or human origin (Kwei et al., 2010). The studies using a pre-osteoblastic cell line reported increased levels of metabolic activity on HA surfaces only at later timepoints, with no difference recorded from days 1 to 7 (Beşkardeş et al., 2015; Kong et al., 2005; Thein-Han & Misra, 2009). In a study using stem cells isolated from adult human bone marrow, the proliferation of cells depended on the concentration of HA used, with higher concentrations of HA eliciting an initial increase in proliferation followed by a sharp decrease as time progressed past 14 days.

The difference in cell morphology seen here on the chitosan-nHA surface as compared to the chitosan-only surface, was also observed for goat bone marrow stromal cells seeded on chitosan-HA freeze-dried scaffolds, with more rounded cells on the chitosan layer compared to a flattened morphology on the HA layer (Oliveira et al., 2006). This effect on cell morphology was also echoed in studies comparing chitosan to chitosan-HA composites using murine MC 3T3-E1 cells (Kong et al., 2005; Thein-Han & Misra, 2009), and points to a difference in the integrin binding ability of HA compared to chitosan, possibly due to the presence of the divalent cation Ca^{2+} in the HA which promotes integrin binding to the substrate (Malafaya & Reis, 2009).

4.5. Scaffold support for stem cell differentiation

MSCs cultured on both scaffolds showed enhanced ALP levels per scaffold at day 14 in osteogenic medium compared to standard culture

medium, indicating these scaffolds supported osteogenic differentiation. An increase in ALP activity in osteogenic medium was also seen in other studies using MSCs cultured on chitosan-HA composite scaffolds (Moreau & Xu, 2009; Oliveira et al., 2006). A later study using MC3T3 pre-osteoblastic cells found similar levels of ALP in cells cultured on chitosan scaffolds with and without HA at day 14; however, at day 7, ALP levels were elevated in the chitosan-HA scaffold (Beşkardeş et al., 2015), indicating osteogenesis is promoted on HA-containing scaffolds. Additional reports on osteogenic differentiation on chitosan-HA scaffolds showed upregulation of osteogenic genetic markers, such as osteopontin (Oliveira et al., 2006), osteonectin and osteocalcin (Kwei et al., 2010). Further evaluation of ALP activity normalised to cellular content over time could help refine the monitoring of osteogenic kinetics in cell-seeded scaffolds.

The ability of the chitosan-only scaffold layer to preferentially support chondrogenesis was indicated by increased levels of GAGs produced on MSC-seeded chitosan-only layers of the scaffold compared to the chitosan-nHA layer of the composite scaffold. A previous study using PLGA scaffolds, containing different levels of HA, cultured in chondrogenic medium showed a decrease in gene expression of chondrogenic markers, such as Collagen X and Sox9, on surfaces with HA (Kwei et al., 2010), indicating downregulated chondrogenesis in the presence of HA.

The results in the present study indicate that the scaffold design can provide support for osteochondral regeneration, with nHA rods solely added to the bone-like layer to favour integration to the subchondral region, and a chitosan-only layer on the surface to promote cartilage repair. Further characterisation of the cellular response, including through the analysis of late lineage markers at the protein and transcript level, will provide more specific information on the range and kinetics of the differentiation achieved within the construct.

5. Conclusion

The chitosan-based composite scaffold developed fulfilled the requirements set out for an osteochondral application. The manufactured construct displayed a controlled porosity and pore size distribution to mimic the natural architecture and chemical composition of osteochondral tissue. The compressive properties have been increased by the incorporation of nHA rods that reinforce the chitosan matrix and provide a higher elastic modulus and stronger structure with thicker, more defined pore walls. The mechanical properties were retained after repeated compressive cycles and importantly, preservation of the internal pore network was confirmed, indicating the scaffold displays excellent mechanical recovery compatible with arthroscopic or minimal invasive surgical delivery. Crucially, the biomimetic stratified structure did not delaminate under tensile loading.

The attachment and proliferation of mesenchymal stem cells was supported by the chitosan scaffold and enhanced by the inclusion of nHA. The distinct chondral-like and osteo-like layers preferentially supported early-stage osteogenesis and chondrogenesis respectively when subjected to differentiation conditions and promoted a phenotype typical of differentiated stem cells. These results indicate the bilayer chitosan/chitosan-nHA composite scaffold is a promising candidate for future osteochondral repair applications. On the basis of the observations presented here, the preclinical analysis of the scaffold in vivo represents the next experimental step to further evaluate its potential.

Supplementary data to this article can be found online at https://doi.org/10.1016/j.carbpol.2022.119126.

Declaration of competing interest

The authors declare that they have no known competing financial interests or personal relationships that could have appeared to influence the work reported in this paper.

Acknowledgements

This work was supported by the UK Engineering and Physical Sciences Research Council (EPSRC) Centre for Doctoral Training [grant number EP/F500491/1], the EPSRC Centre for Innovative Manufacturing for Medical Devices [grant number EP/K029592/1]. This report describes work conducted under the Medical Technologies Innovation and Knowledge Centre's Proof of Concept programme, funded by the EPSRC [grant number POC062]. This work was supported by Versus Arthritis [grant number 21501]. VS is funded by a grant from the Italian Ministry of Education, University and Research (MIUR) to the Department of Molecular Medicine (University of Pavia) under the 'Dipartimenti di Eccellenza (2018–2022)' initiative.

References

Aslam Khan, M. U., Raza, M. A., Mehboob, H., Abdul Kadir, M. R., Abd Razak, S. I., Shah, S. A., Iqbal, M. Z., & Amin, R. (2020). Development and in vitro evaluation of κ-carrageenan based polymeric hybrid nanocomposite scaffolds for bone tissue engineering. *RSC Advances, 10*(66), 40529–40542. https://doi.org/10.1039/D0RA07446B

Beşkardeş, I. G., Demirtaş, T. T., Durukan, M. D., & Gümüşderelioğlu, M. (2015). Microwave-assisted fabrication of chitosan–hydroxyapatite superporous hydrogel composites as bone scaffolds. *Journal of Tissue Engineering and Regenerative Medicine, 9*(11), 1233–1246. https://doi.org/10.1002/term.1677

Bicho, D., Pina, S., Reis, R. L., & Oliveira, J. M. (2018). Commercial products for osteochondral tissue repair and regeneration. In J. M. Oliveira, S. Pina, R. L. Reis, & J. S. Roman (Eds.), *Osteochondral Tissue Engineering: Nanotechnology, Scaffolding-Related Developments and Translation* (pp. 415–428). Cham: Springer International Publishing.

Busilacchi, A., Gigante, A., Mattioli-Belmonte, M., Manzotti, S., & Muzzarelli, R. A. A. (2013). Chitosan stabilizes platelet growth factors and modulates stem cell differentiation toward tissue regeneration. *Carbohydrate Polymers, 98*(1), 665–676. https://doi.org/10.1016/j.carbpol.2013.06.044

Costa-Pinto, A. R., Correlo, V. M., Sol, P. C., Bhattacharya, M., Charbord, P., Delorme, B., Reis, R. L., & Neves, N. M. (2009). Osteogenic differentiation of human bone marrow mesenchymal stem cells seeded on melt based chitosan scaffolds for bone tissue engineering applications. *Biomacromolecules, 10*(8), 2067–2073. https://doi.org/10.1021/bm9000102

Costa-Pinto, A. R., Salgado, A. J., Correlo, V. M., Sol, P., Bhattacharya, M., Charbord, P., Reis, R. L., & Neves, N. M. (2008). Adhesion, proliferation, and osteogenic differentiation of a mouse mesenchymal stem cell line (BMC9) seeded on novel melt-based chitosan/polyester 3D porous scaffolds. *Tissue Engineering Part A, 14*(6), 1049–1057. https://doi.org/10.1089/tea.2007.0153

Croisier, F., & Jérôme, C. (2013). Chitosan-based biomaterials for tissue engineering. *European Polymer Journal, 49*(4), 780–792. https://doi.org/10.1016/j.eurpolymj.2012.12.009

Dang, Q. F., Yan, J. Q., Li, J. J., Cheng, X. J., Liu, C. S., & Chen, X. G. (2011). Controlled gelation temperature, pore diameter and degradation of a highly porous chitosan-based hydrogel. *Carbohydrate Polymers, 83*(1), 171–178. https://doi.org/10.1016/j.carbpol.2010.07.038

Felfel, R. M., Gupta, D., Zabidi, A. Z., Prosser, A., Scotchford, C. A., Sottile, V., & Grant, D. M. (2018). Performance of multiphase scaffolds for bone repair based on two-photon polymerized poly(d, l-lactide-co-ε-caprolactone), recombinamers hydrogel and nano-HA. *Materials & Design, 160*, 455–467. https://doi.org/10.1016/j.matdes.2018.09.035

France, L. A., Scotchford, C. A., Grant, D. M., Rashidi, H., Popov, A. A., & Sottile, V. (2014). Transient serum exposure regimes to support dual differentiation of human mesenchymal stem cells. *Journal of Tissue Engineering and Regenerative Medicine, 8*(8), 652–663. https://doi.org/10.1002/term.1567

Frank, R. M., Cotter, E. J., Hannon, C. P., Harrast, J. J., & Cole, B. J. (2019). Cartilage restoration surgery: Incidence rates, complications, and trends as reported by the american Board of Orthopaedic Surgery Part II candidates. *Arthroscopy: The Journal of Arthroscopic & Related Surgery, 35*(1), 171–178. https://doi.org/10.1016/j.arthro.2018.08.028

Gibson, L. J., & Ashby, M. F. (1997). *Cellular Solids: Structure and Properties* (2 ed.). Cambridge: Cambridge University Press.

Gil Mur, F. J. (2016). 8 - Accelerating mineralization of biomimetic surfaces. In C. Aparicio, & M.-P. Ginebra (Eds.), *Biomineralization and biomaterials* (pp. 267–289). Boston: Woodhead Publishing.

GlobeNewswire. (2018). Histogenics announces top-line results from phase 3 clinical trial. Retrieved from https://www.globenewswire.com/news-release/2018/09/05/1565410/0/en/Histogenics-Announces-Top-Line-Results-From-Phase-3-Clinical-Trial-of-NeoCart-in-Patients-With-Knee-Cartilage-Damage.html.

Harley, B. A., Lynn, A. K., Wissner-Gross, Z., Bonfield, W., Yannas, I. V., & Gibson, L. J. (2010). Design of a multiphase osteochondral scaffold III: Fabrication of layered scaffolds with continuous interfaces. *Journal of Biomedical Materials Research Part A, 92A*(3), 1078–1093. https://doi.org/10.1002/jbm.a.32387

Harrison, R., Markides, H., Morris, R. H., Richards, P., El Haj, A. J., & Sottile, V. (2017). Autonomous magnetic labelling of functional mesenchymal stem cells for improved traceability and spatial control in cell therapy applications. *Journal of Tissue*

Engineering and Regenerative Medicine, 11(8), 2333–2348. https://doi.org/10.1002/term.2133

Hoemann, C. D., Hurtig, M., Rossomacha, E., Sun, J., Chevrier, A., Shive, M. S., & Buschmann, M. D. (2005). Chitosan-glycerol phosphate/blood implants improve hyaline cartilage repair in ovine microfracture defects. *The Journal of Bone and Joint Surgery. American Volume, 87*(12), 2671–2686. https://doi.org/10.2106/jbjs.D.02536

Hughes, S. W. (2005). Archimedes revisited: A faster, better, cheaper method of accurately measuring the volume of small objects. *Physics Education, 40*(5), 468–474. https://doi.org/10.1088/0031-9120/40/5/008

Hui, D., Goodridge, R. D., Scotchford, C. A., & Grant, D. M. (2018). Laser sintering of nano-hydroxyapatite coated polyamide 12 powders. *Additive Manufacturing, 22*, 560–570. https://doi.org/10.1016/j.addma.2018.05.045

Hutmacher, D. W. (2000). Scaffolds in tissue engineering bone and cartilage. *Biomaterials, 21*(24), 2529–2543. https://doi.org/10.1016/S0142-9612(00)00121-6

Iglesias-Mejuto, A., & García-González, C. A. (2021). 3D-printed alginate-hydroxyapatite aerogel scaffolds for bone tissue engineering. *Materials Science and Engineering: C, 131*, Article 112525. https://doi.org/10.1016/j.msec.2021.112525

King, L. K., Waugh, E. J., Marshall, D. A., & Hawker, G. A. (2017). Association between comorbidity and non-surgical treatment of patients with knee osteoarthritis. *Osteoarthritis and Cartilage, 25*, S347–S348. https://doi.org/10.1016/j.joca.2017.02.587

Kon, E., Delcogliano, M., Filardo, G., Pressato, D., Busacca, M., Grigolo, B., Desando, G., & Marcacci, M. (2010). A novel nano-composite multi-layered biomaterial for treatment of osteochondral lesions: Technique note and an early stability pilot clinical trial. *Injury, 41*(7), 693–701. https://doi.org/10.1016/j.injury.2009.11.014

Kon, E., Filardo, G., Brittberg, M., Busacca, M., Condello, V., Engebretsen, L., Marlovits, S., Niemeyer, P., Platzer, P., Posthumus, M., Verdonk, P., Verdonk, R., Victor, J., van der Merwe, W., Widuchowski, W., Zorzi, C., & Marcacci, M. (2017). A multilayer biomaterial for osteochondral regeneration shows superiority vs microfractures for the treatment of osteochondral lesions in a multicentre randomized trial at 2 years. *Knee Surgery, Sports Traumatology, Arthroscopy.*. https://doi.org/10.1007/s00167-017-4707-3

Kong, L., Gao, Y., Cao, W., Gong, Y., Zhao, N., & Zhang, X. (2005). Preparation and characterization of nano-hydroxyapatite/chitosan composite scaffolds. *Journal of Biomedical Materials Research Part A, 75A*(2), 275–282. https://doi.org/10.1002/jbm.a.30414

Kwei, S. P., Moffat, K. L., Doty, S., & Lu, H. H. (2010). Effect of hydroxyapatite particles on stem cell response in nanofiber scaffolds, 26-28 March 2010). In *Paper presented at the proceedings of the 2010 IEEE 36th annual northeast bioengineering conference (NEBEC)*.

Lester, E., Tang, S. V. Y., Khlobystov, A., Rose, V. L., Buttery, L., & Roberts, C. J. (2013). Producing nanotubes of biocompatible hydroxyapatite by continuous hydrothermal synthesis. *CrystEngComm, 15*(17), 3256–3260. https://doi.org/10.1039/C3CE26798A

Levengood, S. L., & Zhang, M. (2014). Chitosan-based scaffolds for bone tissue engineering. *Journal of Materials Chemistry. B, Materials for Biology and Medicine, 2*(21), 3161–3184. https://doi.org/10.1039/c4tb00027g

Malafaya, P. B., & Reis, R. L. (2009). Bilayered chitosan-based scaffolds for osteochondral tissue engineering: Influence of hydroxyapatite on in vitro cytotoxicity and dynamic bioactivity studies in a specific double-chamber bioreactor. *Acta Biomaterialia, 5*(2), 644–660. https://doi.org/10.1016/j.actbio.2008.09.017

Martin, I., Miot, S., Barbero, A., Jakob, M., & Wendt, D. (2007). Osteochondral tissue engineering. *Journal of Biomechanics, 40*(4), 750–765. https://doi.org/10.1016/j.jbiomech.2006.03.008

McCarrel, T. M., Pownder, S. L., Gilbert, S., Koff, M. F., Castiglione, E., Saska, R. A., Bradica, G., & Fortier, L. A. (2017). Two-year evaluation of osteochondral repair with a novel biphasic graft saturated in bone marrow in an equine model. *Cartilage, 8*(4), 406–416. https://doi.org/10.1177/1947603516675913

McCarthy, H. S., & Roberts, S. (2013). A histological comparison of the repair tissue formed when using either Chondrogide® or periosteum during autologous chondrocyte implantation. *Osteoarthritis and Cartilage, 21*(12), 2048–2057. https://doi.org/10.1016/j.joca.2013.10.004

Moreau, J. L., & Xu, H. H. K. (2009). Mesenchymal stem cell proliferation and differentiation on an injectable calcium phosphate – chitosan composite scaffold. *Biomaterials, 30*(14), 2675–2682. https://doi.org/10.1016/j.biomaterials.2009.01.022

Murphy, C. M., Duffy, G. P., Schindeler, A., & O'Brien, F. J. (2016). Effect of collagen-glycosaminoglycan scaffold pore size on matrix mineralization and cellular behavior in different cell types. *Journal of Biomedical Materials Research Part A, 104*(1), 291–304. https://doi.org/10.1002/jbm.a.35567

Muzzarelli, R. A., Mattioli-Belmonte, M., Tietz, C., Biagini, R., Ferioli, G., Brunelli, M. A., Fini, M., Giardino, R., Ilari, P., & Biagini, G. (1994). Stimulatory effect on bone formation exerted by a modified chitosan. *Biomaterials, 15*(13), 1075–1081. https://doi.org/10.1016/0142-9612(94)90093-0

Nath, S. D., Abueva, C., Kim, B., & Lee, B. T. (2015). Chitosan-hyaluronic acid polyelectrolyte complex scaffold crosslinked with genipin for immobilization and controlled release of BMP-2. *Carbohydrate Polymers, 115*, 160–169. https://doi.org/10.1016/j.carbpol.2014.08.077

National Health Service. NHS risk of knee replacements. https://www.nhs.uk/conditions/knee-replacement/risks/. (Accessed 5 January 2020) [Online].

National Institute of Health and Care Excellence. (2019). Nice guidance on musculoskeletal conditions. https://www.nice.org.uk/guidance/conditions-anddiseases/musculoskeletal-conditions/knee-conditions. (Accessed 10 May 2019) [Online].

Nawaz, S. Z., Bentley, G., Briggs, T. W. R., Carrington, R. W. J., Skinner, J. A., Gallagher, K. R., & Dhinsa, B. S. (2014). Autologous chondrocyte implantation in the knee: Mid-term to long-term results. *JBJS, 96*(10), 824–830. https://doi.org/10.2106/jbjs.L.01695

Offeddu, G. S., Tanase, C. E., Toumpaniari, S., Oyen, M. L., & Cameron, R. E. (2018). Stiffening by osmotic swelling constraint in cartilage-like cell culture scaffolds. *Macromolecular Bioscience, 18*(11), 1800247. https://doi.org/10.1002/mabi.201800247

Oliveira, J. M., Rodrigues, M. T., Silva, S. S., Malafaya, P. B., Gomes, M. E., Viegas, C. A., Dias, I. R., Azevedo, J. T., Mano, J. F., & Reis, R. L. (2006). Novel hydroxyapatite/chitosan bilayered scaffold for osteochondral tissue-engineering applications: Scaffold design and its performance when seeded with goat bone marrow stromal cells. *Biomaterials, 27*(36), 6123–6137. https://doi.org/10.1016/j.biomaterials.2006.07.034

Pati, F., Adhikari, B., & Dhara, S. (2012). Development of chitosan-tripolyphosphate non-woven fibrous scaffolds for tissue engineering application. *Journal of Materials Science. Materials in Medicine, 23*(4), 1085–1096. https://doi.org/10.1007/s10856-012-4559-9

Reddy, M. S. B., Ponnamma, D., Choudhary, R., & Sadasivuni, K. K. (2021). A comparative review of natural and synthetic biopolymer composite scaffolds. Retrieved from *Polymers, 13*(7), 1105 https://www.mdpi.com/2073-4360/13/7/1105.

Ren, D., Yi, H., Wang, W., & Ma, X. (2005). The enzymatic degradation and swelling properties of chitosan matrices with different degrees of N-acetylation. *Carbohydrate Research, 340*(15), 2403–2410. https://doi.org/10.1016/j.carres.2005.07.022

Roberts, G. A. F. (1992). *Chitin chemistry*, 26-28 March 2010) (Vol. 1). London Macmillian.

Sarem, M., Moztarzadeh, F., & Mozafari, M. (2013). How can genipin assist gelatin/carbohydrate chitosan scaffolds to act as replacements of load-bearing soft tissues? *Carbohydrate Polymers, 93*(2), 635–643. https://doi.org/10.1016/j.carbpol.2012.11.099

Schneider, U., Rackwitz, L., Andereya, S., Siebenlist, S., Fensky, F., Reichert, J., Loer, I., Barthel, T., Rudert, M., & Noth, U. (2011). A prospective multicenter study on the outcome of type I collagen hydrogel-based autologous chondrocyte implantation (CaReS) for the repair of articular cartilage defects in the knee. *The American Journal of Sports Medicine, 39*(12), 2558–2565. https://doi.org/10.1177/0363546511423369

Siddiqui, N., Pramanik, K., & Jabbari, E. (2015). Osteogenic differentiation of human mesenchymal stem cells in freeze-gelled chitosan/nano beta-tricalcium phosphate porous scaffolds crosslinked with genipin. *Materials Science & Engineering. C, Materials for Biological Applications, 54*, 76–83. https://doi.org/10.1016/j.msec.2015.05.005

Stanish, W. D., McCormack, R., Forriol, F., Mohtadi, N., Pelet, S., Desnoyers, J., Restrepo, A., & Shive, M. S. (2013). Novel scaffold-based BST-CarGel treatment results in superior cartilage repair compared with microfracture in a randomized controlled trial. *The Journal of Bone and Joint Surgery. American Volume, 95*(18), 1640–1650. https://doi.org/10.2106/jbjs.l.01345

Thein-Han, W. W., & Misra, R. D. (2009). Biomimetic chitosan-nanohydroxyapatite composite scaffolds for bone tissue engineering. *Acta Biomaterialia, 5*(4), 1182–1197. https://doi.org/10.1016/j.actbio.2008.11.025

Tindall, G. W., Perry, R. L., & Spaugh, A. T. (1994). *Depolymerization of Substantially Amorphous Polyesters*. Canada Patent No. CA2145747A1 [online: accessed 11-10-20] https://patents.google.com/patent/CA2145747A1/en.

Vårum, K. M., Myhr, M. M., Hjerde, R. J. N., & Smidsrød, O. (1997). In vitro degradation rates of partially N-acetylated chitosans in human serum. *Carbohydrate Research, 299*(1), 99–101. https://doi.org/10.1016/S0008-6215(96)00332-1

Viala, S., Freche, M., & Lacout, J. L. (1996). Effect of chitosan on octacalcium phosphate crystal growth. *Carbohydrate Polymers, 29*(3), 197–201. https://doi.org/10.1016/0144-8617(96)00023-9

Wu, F., Pang, Y., & Liu, J. (2020). Swelling-strengthening hydrogels by embedding with deformable nanobarriers. *Nature Communications, 11*(1), 4502. https://doi.org/10.1038/s41467-020-18308-9

Xiao, H., Huang, W., Xiong, K., Ruan, S., Yuan, C., Mo, G., Tian, R., Zhou, S., She, R., Ye, P., Liu, B., & Deng, J. (2019). Osteochondral repair using scaffolds with gradient pore sizes constructed with silk fibroin, chitosan, and nano-hydroxyapatite. *International Journal of Nanomedicine, 14*, 2011–2027. https://doi.org/10.2147/IJN.S191627

Yadav, M., Goswami, P., Paritosh, K., Kumar, M., Pareek, N., & Vivekanand, V. (2019). Seafood waste: A source for preparation of commercially employable chitin/chitosan materials. *Bioresources and Bioprocessing, 6*(1), 8. https://doi.org/10.1186/s40643-019-0243-y

Yan, L. P., Wang, Y. J., Ren, L., Wu, G., Caridade, S. G., Fan, J. B., Wang, L. Y., Ji, P. H., Oliveira, J. M., Oliveira, J. T., Mano, J. F., & Reis, R. L. (2010). Genipin-cross-linked collagen/chitosan biomimetic scaffolds for articular cartilage tissue engineering applications. *Journal of Biomedical Materials Research. Part A, 95*(2), 465–475. https://doi.org/10.1002/jbm.a.32869

Zhang, T., Zhang, H., Zhang, L., Jia, S., Liu, J., Xiong, Z., & Sun, W. (2017). Biomimetic design and fabrication of multilayered osteochondral scaffolds by low-temperature deposition manufacturing and thermal-induced phase-separation techniques. *Biofabrication, 9*(2), 025021. https://doi.org/10.1088/1758-5090/aa7078

Zhang, B., Huang, J., & Narayan, R. J. (2020). Gradient scaffolds for osteochondral tissue engineering and regeneration. *Journal of Materials Chemistry B, 8*(36), 8149–8170. https://doi.org/10.1039/D0TB00688B

Zou, K., Wong, J., Abdullah, N., Chen, X., Smith, T., Doherty, M., & Zhang, W. (2016). Examination of overall treatment effect and the proportion attributable to contextual effect in osteoarthritis: Meta-analysis of randomised controlled trials. *Annals of the*

Rheumatic Diseases, 75(11), 1964–1970. https://doi.org/10.1136/annrheumdis-2015-208387